Computers in Biology and Medicine 75 (2016) 243–256

Contents lists available at ScienceDirect

Computers in Biology and Medicine

journal homepage: www.elsevier.com/locate/cbm

Towards an SEMG-based tele-operated robot for masticatory rehabilitation

Hadi Kalani [a,c], Sahar Moghimi [a,b,d], Alireza Akbarzadeh [a,c,*]

[a] Center of Excellence on Soft Computing and Intelligent Information Processing, Ferdowsi University of Mashhad, Mashhad, Iran
[b] Rayan Center for Neuroscience and Behavior, Ferdowsi University of Mashhad, Mashhad, Iran
[c] Mechanical Engineering Department, Ferdowsi University of Mashhad, Mashhad, Iran
[d] Electrical Engineering Department, Ferdowsi University of Mashhad, Mashhad, Iran

ARTICLE INFO

Article history:
Received 24 February 2016
Received in revised form
17 May 2016
Accepted 21 May 2016

Keywords:
Clenching movement
SEMG-based control
Rehabilitation robot
Fuzzy impedance control
Fast orthogonal search
Laguerre estimation technique
Artificial neural networks

ABSTRACT

This paper proposes a real-time trajectory generation for a masticatory rehabilitation robot based on surface electromyography (SEMG) signals. We used two Gough-Stewart robots. The first robot was used as a rehabilitation robot while the second robot was developed to model the human jaw system. The legs of the rehabilitation robot were controlled by the SEMG signals of a tele-operator to reproduce the masticatory motion in the human jaw, supposedly mounted on the moving platform, through predicting the location of a reference point. Actual jaw motions and the SEMG signals from the masticatory muscles were recorded and used as output and input, respectively. Three different methods, namely time-delayed neural networks, time delayed fast orthogonal search, and time-delayed Laguerre expansion technique, were employed and compared to predict the kinematic parameters. The optimal model structures as well as the input delays were obtained for each model and each subject through a genetic algorithm. Equations of motion were obtained by the virtual work method. Fuzzy method was employed to develop a fuzzy impedance controller. Moreover, a jaw model was developed to demonstrate the time-varying behavior of the muscle lengths during the rehabilitation process. The three modeling methods were capable of providing reasonably accurate estimations of the kinematic parameters, although the accuracy and training/validation speed of time-delayed fast orthogonal search were higher than those of the other two aforementioned methods. Also, during a simulation study, the fuzzy impedance scheme proved successful in controlling the moving platform for the accurate navigation of the reference point in the desired trajectory. SEMG has been widely used as a control command for prostheses and exoskeleton robots. However, in the current study by employing the proposed rehabilitation robot the complete continuous profile of the clenching motion was reproduced in the sagittal plane.

1. Introduction

Human mastication is a complex process which consists of two movements: clenching and grinding. In clenching the mandible moves only in the sagittal plane, whereas in grinding, it traces a circular path in the frontal plane. Although more than 20 muscles are involved in the process of human mastication, only six of these muscles play the major role [1–4]. For clenching, the Masseter and Temporalis muscles are mostly employed, whereas Pterygoid muscles have the main role in grinding. The movement of human jaw has been investigated by a variety of methods [5–7]. Also, different methods have been utilized for motion classification, e.g. Bayesian classifier [5], artificial neural networks [8–12] and fast orthogonal search (FOS) [13]. Surface electromyography (SEMG) has been used to identify differences in chewing patterns between individuals, and to classify them into groups according to their chewing efficiency [14–18].

The relationship between muscles' electrical activity and body movements is of special importance in many applications including motion classification, control of prosthetic limbs, and tele-operated robots [19–23]. In these applications, use of non-expensive and portable SEMG electrodes is advantageous compared to the use of sensors and cameras which are often very expensive and require massive structures [24]. Generally, SEMG based control is a complex technique which involves detection, processing, and classification for different applications including assistive robots [25,26]. All the SEMG processing methods belong to one of the three main categories: time, frequency, and time-frequency domain processing [19]. Moreover, signal classification is a basic

* Corresponding author at: Department of Mechanical Engineering, Ferdowsi University of Mashhad, Mashhad 9177948974, Iran.
E-mail address: s.moghimi@um.ac.ir (S. Moghimi).

http://dx.doi.org/10.1016/j.compbiomed.2016.05.014
0010-4825/

step in SEMG based control in a way that accuracy of the control strategy depends highly on the method of classification [27–35]. Robots use different techniques for signal classification, e.g. artificial neural networks [28,29], fuzzy logic [30], neuro-fuzzy methods [27–31] and support vector machines [34,35].

Disorders associated with mastication, e.g. temporomandibular disorders (TMD), craniomandibular disorders (CMD), trismus and edentulous maxilla [36,37], can directly influence many aspects of a patient's life by reducing his/her ability to open the mouth. Different strategies are adopted for the treatment of these disorders. An ordinary manual rehabilitation session often involves difficult maneuvers with force imposed at specific points along a predefined direction of the movement. This method highly depends on the doctor's skills, and may not always be convenient for long-term post-operative physiotherapy [38–47]. Numerical modeling (e.g. finite element method) may provide valuable insight about the stress distribution during the physiotherapy protocol [48,49].

Stretching techniques and jaw-mobilizing devices/robots are available for rehabilitation purposes [38,39]. Studies show that continuous and passive exercise therapy can be effective for pain reduction caused by musculoskeletal deficiencies during jaw movement [38–42]. Recently, robotic systems, including the TheraBite System [42,43], the Dynasplint_Trismus System [47] and the WY (Waseda-Yamanashi) series of robots [44,45], have been employed in clinics for rehabilitation purposes. Generally, the ability of robots to produce repetitive movements and permitting programmable rehabilitation sessions with varying intensity make them helpful tools for conducting effective rehabilitation strategies [41].

In a rehabilitation robot, the volunteer is part of a man-machine system and his/her dynamic model is not as clear and invariant as that of the manipulator [50–57]. Controller design is one of the main complications in employing rehabilitation robots. In this regard, the impedance control scheme was introduced by Hogan [58]. Using this method enables the operator to assign the desired mass/inertia, damping, and stiffness to the robot. The most important feature of impedance control is handling constrained and unconstrained motion [59]. In this method the robot is modeled as a mass, spring, and damper in interaction with human or environment. This type of impedance control is usually called pure impedance control [60] using which external force (applied by human and/or environment) is not controlled. This force can cause serious issues considering the safety of patients. To eliminate this problem, researchers have introduced force tracking impedance control [58–63].

In this study instead of designing a robot that mimics the human masticatory process, we propose a Gough-Stewart robot which is controlled by the SEMG signals of a tele-operator. The robot legs were controlled to reproduce the masticatory process in the human jaw, supposedly mounted on the moving platform, through predicting the location of a reference point (the chin point (CP), placed on the end effector of the rehabilitation robot) using SEMG signals. To the best of our knowledge, this is the first time that a continuous profile of the masticatory motion is predicted and reproduced by a robot. The aforementioned robot was utilized as a rehabilitation robot and equations of motion were obtained by the virtual work method. Fuzzy method was employed to develop a hybrid position/force fuzzy impedance control [62]. Moreover, a jaw model was developed by a general Gough-Stewart parallel robot to demonstrate the time-varying behavior of the muscle lengths of subjects in the rehabilitation process. The proposed approach enables the tele-operator to reproduce the required masticatory motion in the patient's jaw through opening/closing of his mouth to the desired extent.

2. Materials and methods

2.1. Experimental setup and procedure

In this work, three kinematic parameters (displacement along the x and z axes and rotation about the y-axis) were predicted using SEMG signals and utilized in the control scheme for reproducing the masticatory trajectory. Seven volunteers (four males) participated in this study. All subjects were well-informed about the procedure and provided written consent to the experimental protocol. In each trial, volunteers were asked to perform a maximum voluntary mandible opening and closing (clenching movement) in the sagittal plane within an interval of five seconds [12]. Three trials were used for training and another three trials were employed for model validation. To record the electrical activity of muscles, an 8-channel SEMG system was employed. For each subject SEMG signals were recorded from four muscles, namely right and left Masseter, and right and left Temporalis muscles (Fig. 1). Recorded raw SEMG signals were passed through a band pass (15–400 Hz) 3rd order Butterworth filter. The resulted signals were rectified and smoothed by a moving average window of size 200. The sampling rate was reduced to 250 Hz. Moreover, to trace the chewing trajectory, Simi Reality Motion System (GmbH, Germany) was employed. The camera output was digitized to 250 frames per second (fps). Frequencies above 7 Hz were removed.

2.2. SEMG-based motion prediction

Different delays of the SEMG signals from the Temporalis and Masseter muscles were used as inputs since it was necessary to consider the delay between muscle activation and limb movements. This delay is variable, depends on several factors including the firing rate dynamics of the muscle, and cannot be neglected [73,74]. This Electromechanical delay has been reported to range from 10 ms to about 100 ms [74–76]. Kinematic variables (i.e.,

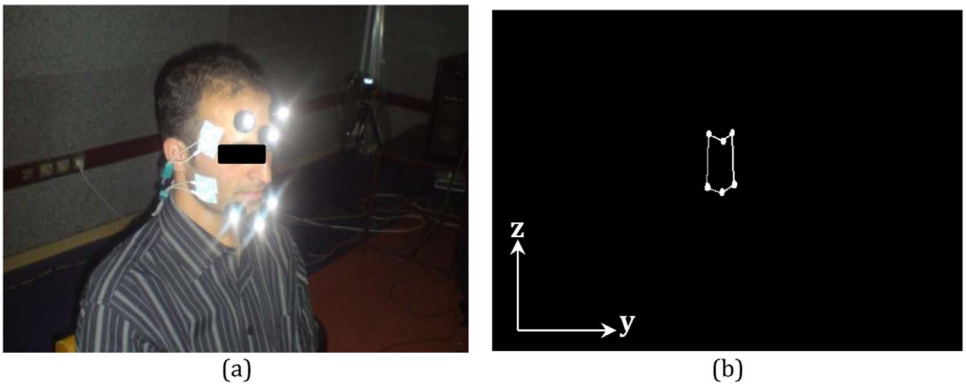

Fig. 1. (a) Marker position and SEMG electrodes on the subject's face. (b) Two-dimensional reconstruction of the marker set.

position of the CP along the x- and z-axes, and rotation about the y-axis) were set as outputs. Three methods were developed for predicting the desired outputs: time-delayed multi-layered perceptron artificial neural network (TDMLPANN), time-delayed fast orthogonal search (TDFOS), and time-delayed Laguerre expansion technique (TDLET). The performance of the aforementioned methods were compared to seek out the fastest and most efficient approach to be employed in the real time tele-operation task.

2.2.1. TDMLPANN

Generally, TDMLPANN is known as a universal approximator for nonlinear input-output mapping. Here, nodes of the hidden and output layers had log-sigmoidal and purely linear transfer functions, respectively. Three TDMLPANN were trained for predicting the position/orientation (x_{CP}, z_{Cp} and β) based on different delays of the SEMG signals. Weights and biases of the network were initialized with random values. Batch training was used, in which the weights between neurons were updated only after the network was exposed to all the training samples. The Levenberg-Marquardt method which gave the best possible results was used for training [12].

2.2.2. TDFOS

In 1985 Korenberg introduced FOS [64,65]. The main goal of this method is to minimize the mean-square error (MSE) of estimation by choosing the best basis functions among all candidates (including polynomial, square and sigmoid functions), which cause the maximum reduction in the mean square difference between estimated and measured data. Korenberg proposed an efficient method to obtain the coefficients corresponding to the selected basis functions. In this paper, four kinds of basis functions (common, squared, quadratic and sigmoid functions) were employed considering different delays of the inputs, hence the name TDFOS [13]. Table 1 summarizes these functions. Employing the FOS method we have

$$y(n)=\sum_{m=1}^{M} a_m p_m(n)+e(n) \tag{1}$$

where $y(n)$ is the measured output, $e(n)$ is the prediction error and $\sum_{m=1}^{M} a_m p_m(n)$ is the estimated output. Additionally $p_m(n)$ and a_m are the selected basis functions and their corresponding coefficients, respectively. The FOS method searches through a number, N, of available candidate functions, where $N >> M$ and iteratively selects those functions with the most contribution in reducing the MSE. A detailed overview of the FOS algorithm is provided in our previous work [13].

2.2.3. TDLET

LET is the best approach for Volterra kernel estimation. This method uses a set of discrete, normalized and orthogonal Laguerre functions, $b_j(m)$, to estimate the Volterra kernels. The Laguerre functions have an exponential behavior, are orthogonal from zero to infinity, and take $x(n)$ as input and translate it to $v_j(n)$ by discrete-time convolution (Fig. 2) [66–68].

The output of the discrete Volterra model can be calculated as follows

$$y(n)=c_0+\sum_{r=1}^{Q}\sum_{j_1=1}^{L}\sum_{j_r=1}^{j_{r-1}} c_r(j_1,\ldots,j_r)v_{j_1}(n)\ldots v_{j_r}(n)+\varepsilon(n) \tag{2}$$

where $y(n)$ is the output, L is the number of filters, $\varepsilon(n)$ is the estimation residue and c_r represents the polynomial coefficients. Detailed description of LET is provided in our previous work [67]. TDLET is similar to LET except for the fact that inputs to the filter bank consist of different delays of the SEMG signals from the Masseter and Temporalis muscles.

Table 1
List of basis functions. E_{Ma} and E_{Te} are the SEMG signals of the Masseter and Temporalis muscles, respectively. $E_{Ma(d)}$ and $E_{Te(d)}$ represent the delayed version of the SEMG signals.

Common functions	
Offset	E_{Te}
E_{Ma}	$E_{Te(d)}$
$E_{Ma(d)}$	$E_{Ma}*E_{Te}$
$E_{Ma}*E_{Ma(d)}$	$E_{Ma(d)}*E_{Te}$
$E_{Ma}*E_{Te(d)}$	$E_{Ma(d)}*E_{Te(d)}$
$E_{Te}*E_{Te(d)}$	
Squared functions	
$\sqrt{E_{Ma}}$	$\sqrt{E_{Te}}$
$\sqrt{E_{Ma(d)}}$	$\sqrt{E_{Te(d)}}$
$\sqrt{E_{Ma}*E_{Ma(d)}}$	$\sqrt{E_{Ma}*E_{Te}}$
$\sqrt{E_{Ma}*E_{Te(d)}}$	$\sqrt{E_{Ma(d)}*E_{Te}}$
$\sqrt{E_{Te}*E_{Te(d)}}$	$\sqrt{E_{Ma(d)}*E_{Te(d)}}$
Quadratic functions	
$E_{Ma}*E_{Ma}$	$E_{Ma(d)}*E_{Ma(d)}$
$E_{Te(d)}*E_{Te(d)}$	$E_{Te}*E_{Te}$
Sigmoid functions	
$\mathrm{sigm}(E_{Ma})$	$\mathrm{sigm}(E_{Te})$
$\mathrm{sigm}(E_{Ma(d)})$	$\mathrm{sigm}(E_{Te(d)})$
$\mathrm{sigm}(E_{Ma})*\mathrm{sigm}(E_{Ma(d)})$	$\mathrm{sigm}(E_{Ma})*\mathrm{sigm}(E_{Te})$
$\mathrm{sigm}(E_{Ma})*\mathrm{sigm}(E_{Te(d)})$	$\mathrm{sigm}(E_{Ma(d)})*\mathrm{sigm}(E_{Te})$
$\mathrm{sigm}(E_{Te})*\mathrm{sigm}(E_{Te(d)})$	$\mathrm{sigm}(E_{Ma(d)})*\mathrm{sigm}(E_{Te(d)})$

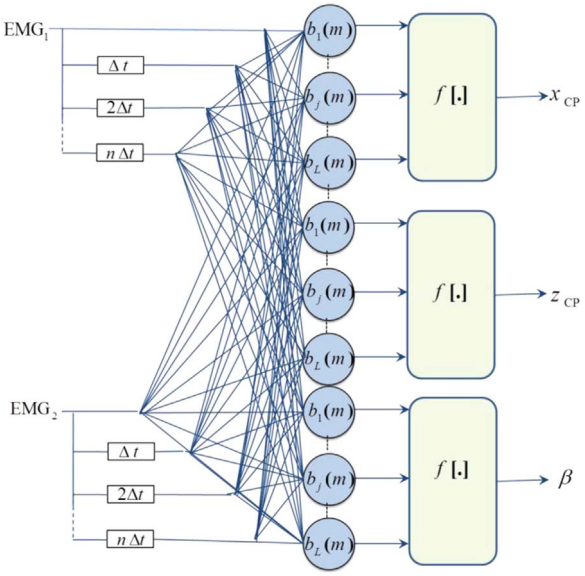

Fig. 2. Schematic of TDLET. $b_j(\mathrm{m})$ is the discrete Laguerre function of order j and m varies between 1 and M (system memory). f [.] is a nonlinear function of order Q.

2.2.4. Choosing the optimal parameters

For each of the three methods employed for modeling the trajectory related parameters, there are a few degrees of freedom which determine the structure and complexity of the developed model. We employed the Genetic Algorithm (GA) to find the best structures and reference inputs for the prediction process. The TDMLPANN, TDFOS and TDLET searched for the best nonlinear mapping function to predict the targets (kinematic variables), based on the structural parameters provided by the GA. The structural parameters to be determined were: for TDMLPANN, the

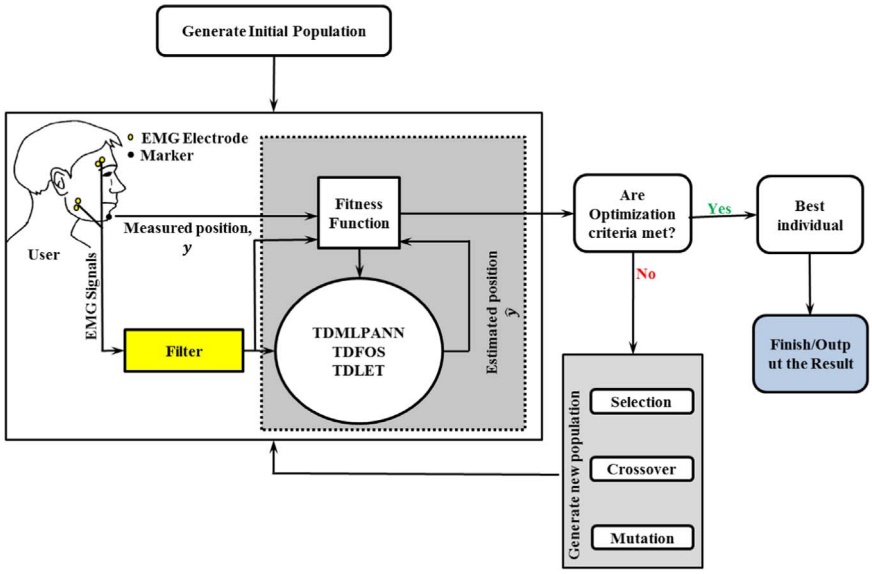

Fig. 3. Block diagram of the proposed technique for choosing the optimal parameters.

number of hidden layers (1 or 2 layers) and the number of neurons in each hidden layer (5–30); for TDFOS, the number of basis functions (2–30); and for TDLET, the number of filters in the filter bank (2–8) and the rate of exponential decline (0.1–0.8). Input delays were restricted to 0–100 ms (with 20-ms intervals) [12]. Fig. 3 shows the proposed algorithm. Optimal parameters of the aforementioned models were separately computed for each subject. After finding the optimal model structure three evaluation criteria were used to validate the developed models: namely, the relative mean square error (RMSE), cross-correlation (CC), and average absolute error (AAE).

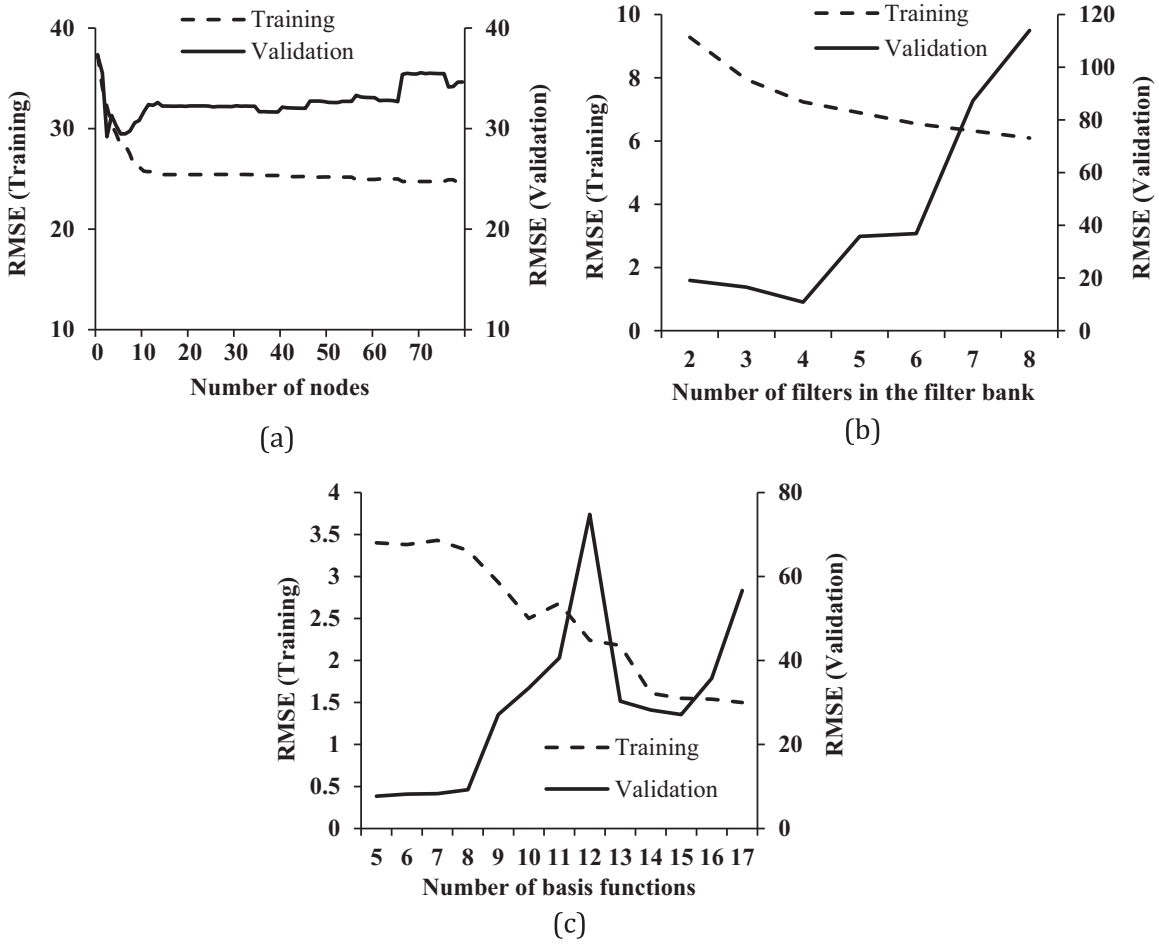

Fig. 4. Effect of varying the (a) number of neurons, (b) filters in the filter banks and (c) basis functions in training and validation on RMSE.

$$\mathrm{RMSE} = 100*\frac{\sum_i \left(y_i - \hat{y}_i\right)^2}{\sum_i (y_i)^2} \tag{3}$$

$$\mathrm{CC} = 100*\frac{\sum_i \left(y_i * \hat{y}_i\right)}{\sqrt{\sum_i (y_i)^2}\sqrt{\sum_i (\hat{y}_i)^2}} \tag{4}$$

$$\mathrm{AAE} = \frac{\sum_i \left|y_i - \hat{y}_i\right|}{n} \tag{5}$$

where n is the number of samples. The proposed system was trained with the first 50% of the recorded data (three trials), while validation was performed with the three remaining trials.

Fig. 4 shows the effect of changing the number of neurons, basis functions, and filters of the filter banks in the RSME value of trainings and validation steps, for TDMLPANN, TDFOS and TDLET, respectively. As shown in Fig. 4, an increase in these parameters resulted in reduced training RMSE values. However, during the validation phase extensive increase of the aforementioned parameters caused high error values. This demonstrates the occurrence of the phenomenon overtraining. Therefore, as indicated by these figures to avoid overtraining and to find the best architecture for each model and subject, employing an optimization method seems plausible. Otherwise, tiresome trials are required to seek out the best structure for achieving the minimum prediction error.

2.3. Rehabilitation robot and Jaw model

Our rehabilitation robot consisted of a moving platform which produced the masticatory motion in the patient's jaw, supposedly fixed on the platform. The motion was a reproduction of the masticatory process, recorded and reproduced based on the SEMG signals (using methods introduced in Section 2.2) of a tele-operator. Both the rehabilitation robot and jaw model were developed using a Gough-Stewart platform. The Gough-Stewart platform is a parallel manipulator, which consists of a mobile platform and a stationary base, connected to each other by six linear actuators. For the rehabilitation robot the 6 linear legs were placed between the moving platform (with the jaw model on top of it) and ground. In the jaw model each of the major chewing muscles (Masseter, Temporalis, and Pterygoid) was modeled using a linear actuator. The mobile and stationary platforms represented the human jaw and skull, respectively. The jaw model was developed merely to illustrate how the platform movements affected the masticatory muscles in the human jaw. Table A1.1 (Appendix A.1) and Table A2.1 (Appendix A.2) summarize the parameters of jaw model and rehabilitation robot, respectively.

For real-time evaluation of the interaction between the rehabilitation robot and human jaw we developed a robot simulator in SimMechanic R2012b. This simulator generated the variations in leg lengths of both the jaw model and rehabilitation robot, and hence reproduced the movement of the robot platform as well as the masticatory motion (Fig. 5). All the modeling and control strategies were developed based on the position of the CP illustrated in Fig. 5.

The dynamic equations of the Gough-Stewart model were obtained by the virtual work method. This method allows elimination of the constraint forces/moments at the passive joints from the equations of motion [69,71]. Since, the dynamic formulations are derived in the joint space, the concept of direct link Jacobian matrices were employed to obtain all rigid bodies' twists. The direct link Jacobian matrices convert the twist of the rigid bodies to actuated joint velocities. Using the principles of virtual work the equations of motion of the robot can be expressed as

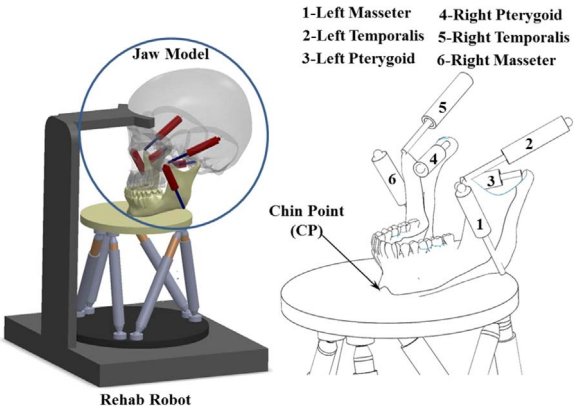

Fig. 5. Architecture of the simulator.

$$\left(\delta\mathbf{q}^{\mathrm{ac}}\right)^{\mathrm{T}}\mathbf{f}^{\mathrm{ac}}+\left(\delta\mathbf{t}_{\mathrm{MP}}\right)^{\mathrm{T}}\mathbf{w}_{\mathrm{MP}}+\sum_{i=1}^{6}\left(\left(\delta^{\mathcal{F}i}\mathbf{t}_{\mathrm{cyl},i}\right)^{\mathrm{T}}{}^{\mathcal{F}i}\mathbf{w}_{\mathrm{cyl},i}+\left(\delta^{\mathcal{F}i}\mathbf{t}_{\mathrm{pis},i}\right)^{\mathrm{T}}{}^{\mathcal{F}i}\mathbf{w}_{\mathrm{pis},i}\right)=0 \tag{6}$$

where $\delta\mathbf{q}^{\mathrm{ac}}$ is the virtual translational vector of the actuated joints, $\mathbf{w}_{\mathrm{MP}}$ represents applied external wrench and inertia of the moving platform, and ${}^{\mathcal{F}i}\mathbf{w}_{\mathrm{cyl},i}$ and ${}^{\mathcal{F}i}\mathbf{w}_{\mathrm{pis},i}$ are resultant wrench due to inertia of the cylinder and piston of i^{th} actuators in its local frame $\{\mathcal{F}_i\}$, respectively. Moreover, $\delta\mathbf{t}_{\mathrm{MP}}$ is the virtual twist vector of the moving platform and $\mathbf{f}^{\mathrm{ac}}$is the actuated joints force. Furthermore, $\delta^{\mathcal{F}i}\mathbf{t}_{\mathrm{cyl},i}$ and $\delta^{\mathcal{F}i}\mathbf{t}_{\mathrm{pis},i}$ are the virtual twist vector for cylinder and piston of the i^{th} leg, respectively. By using kinematic equations and Jacobian matrix [69,71], the dynamics are describe as

$$\mathbf{f}^{\mathrm{ac}}+\mathbf{M}(\mathbf{q})\ddot{\mathbf{q}}^{\mathrm{ac}}_{3\times1}+\mathbf{C}(\mathbf{q},\dot{\mathbf{q}})\dot{\mathbf{q}}^{\mathrm{ac}}+\mathbf{G}(\mathbf{q})+\mathbf{w}=0_{6\times1} \tag{7}$$

where, $\mathbf{M}(\mathbf{q})$ is the 6×6 positive definite inertia matrix, $\mathbf{C}(\mathbf{q},\dot{\mathbf{q}})$ is the 6×1 matrix related to centrifugal and Coriolis terms, $\mathbf{G}(\mathbf{q})$ and $\mathbf{w}$ are 6×1 matrices related to gravity vectors of moving platform/robot legs and applied external wrench exerted to moving platform, respectively. $\mathbf{f}^{\mathrm{ac}}$is a 6×1 matrix of input forces.

2.4. SEMG-based fuzzy impedance control

Using the developed control scheme we aimed to tele-operate the rehabilitation robot in real-time. Fig. 6 summarizes the overall framework of the proposed method in the two prediction and control steps. In the first step, two bipolar SEMG electrodes recorded the electrical activity of the Masseter and Temporalis muscles. Next the model predicted the corresponding position/orientation of the subject's mandible (CP) using the processed SEMG signals. Later, in the second step a control law was applied to the robot actuators to move the platform with the purpose of following the predicted trajectory. The controller and force vectors were defined at the location of CP.

The controller consisted of three parts: a PID controller, an impedance filter, and a fuzzy block [62]. For the application introduced in this work a reference force was required for safety issues (to limit the maximum applied force). A reference force cannot be achieved by pure impedance control [62,72]. The fuzzy logic block was used to adjust the gain of the impedance filter around the reference force. Using surface electrodes we were only able to record the activity patterns of the Masseter and Temporalis muscles [12] and these muscles are mostly involved in the clenching movement in the sagittal plane. Therefore, the gain of the impedance filter was only adjusted in the sagittal plane and the reference force was defined along the z-direction.

First, the inverse kinematics problem of the robot was solved

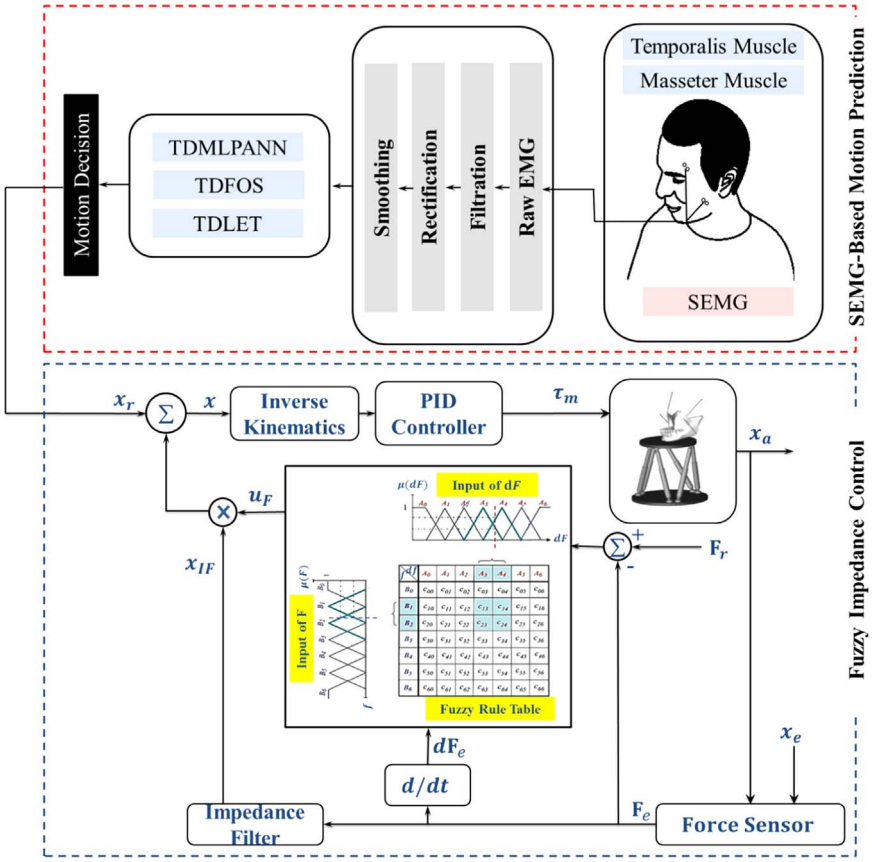

Fig. 6. The overall framework of the proposed online controller. x is the modified trajectory. x_r is the reference trajectory (predicted trajectory based on the SEMG signals). F_e is the applied external force. F_r is the reference force. $\mathbf{x}_{IF}$ represents the impedance filter output. u_F is the fuzzy output and $d\mathbf{F}_e$ represents changes in the applied external force.

for the modified trajectory, $\mathbf{x}$, (also dependent on the fuzzy impedance controller) to determine the corresponding leg lengths (Fig. 6). The leg lengths were controlled by a PID controller. The output of the impedance filter multiplied by the output of the fuzzy block, hereafter called fuzzy impedance output, was used to produce the modified trajectory written as

$$\mathbf{x}=\mathbf{x}_r+\mathbf{x}_{IF}\times u_F\times(\mathbf{F}_r-\mathbf{F}_e,\ d\mathbf{F}_e)\times\mathbf{F}_e \tag{8}$$

where $\mathbf{x}$ is the modified trajectory. $\mathbf{x}_r$ is the reference trajectory (predicted trajectory based on the SEMG signals). $\mathbf{F}_e$ and $\mathbf{F}_r$ are the applied external and reference force, respectively. $\mathbf{x}_{IF}$ represents the impedance filter output. u_F is the fuzzy output and $d\mathbf{F}_e$ represents changes in the applied external force.

The fuzzy Impedance control scheme is a loop which can be added to the robot position controller. As indicated in Fig. 6 the reference trajectory was followed by the PID controller unless external force was applied to the force sensor (otherwise the impedance filter output was 0, since $\boldsymbol{F}_e$=0). When robot interacted with human or environment, external force was applied to the force sensor. The force sensor was modeled as [60]

$$\mathbf{F}_e = \mathbf{K}_e(\mathbf{x}_a - \mathbf{x}_e) \tag{9}$$

where $\mathbf{K}_e$, $\mathbf{x}_a$, and $\mathbf{x}_e$ represent stiffness, actual and allowed trajectory, respectively. If the robot was in contact with any surface, the reference trajectory was modified by the fuzzy impedance output. The following impedance control was applied to obtain the external force vector $\mathbf{F}_e$

$$\mathbf{F}_e=\mathbf{M}(\ddot{\mathbf{x}}_a-\ddot{\mathbf{x}}_r)+\mathbf{B}\left(\dot{\mathbf{x}}_a-\dot{\mathbf{x}}_r\right)+\mathbf{K}(\mathbf{x}_a-\mathbf{x}_r) \tag{10}$$

where $\ddot{\mathbf{x}}_r$, $\dot{\mathbf{x}}_r$ and $\mathbf{x}_r$ are the reference acceleration, velocity and position vectors, respectively. $\mathbf{M}$ is the virtual mass matrix. $\mathbf{B}$and $\mathbf{K}$ are the virtual damping coefficient and spring constant matrices, respectively. Eq. (10) can be expressed in the frequency domain

$$X_a(s)-X_r(s)=Z(s)F(s) \tag{11}$$

where $Z(s)=\frac{1}{Ms^2+Bs+K}$. The impedance filter, $Z(s)$, updated the position of the robot given by Eq. (10). Table 2 summarizes the control parameters. These values were obtained after several trial and error simulations.

For the fuzzy controller, a Mamdani Max–Min, with 2 inputs (force error and rate of force) and one output (filter gain) was used. Seven membership functions for each input and output were chosen. Therefore, overall we had 49 rules. These rules are summarized in Table 3. Moreover, Fig. 7 indicates the membership functions for two inputs and one output. Rules and number of membership functions were selected according to trial and error simulations.

Table 2
Control parameters.

Controller	Parameter	Value
Impedance	$\mathbf{M}$ (N s^2/m)	1
	$\mathbf{B}$ (N s/m)	50
	$\mathbf{K}$ (N/m)	600
	$\mathbf{K_e}$ (N/m)	1000
PID	K_p	3000
	K_i	200
	K_d	500

Table 3
Fuzzy controller rules.

		Rate of force						
		nl	**nm**	**ns**	**z**	**ps**	**pm**	**pl**
Force error	**nl**	z	ns	nm	nl	nl	nl	nl
	nm	z	z	ns	nm	nl	nl	nl
	ns	z	z	Z	ns	ns	nm	nl
	z	pl	pm	ps	z	ns	nm	nl
	ps	pl	pm	ps	ps	z	z	z
	pm	pl	pl	pm	pm	ps	z	z
	pl	pl	pl	pl	pl	pm	ps	z

3. Results

Due to the symmetric role of the aforementioned muscles of healthy subjects in the defined task, the data obtained from the right Temporalis and Masseter muscles were used to predict displacement and orientation.

3.1. SEMG based motion prediction

Fig. 8 shows the ability of three TDMLPANNs, TDFOSs and TDLETs in predicting position/orientation, from the SEMG recordings of one of the subjects. The three columns (from left to right) represent variations in x, z and β-variables, respectively. In general, TDFOS performed better compared to the other methods in predicting the three kinematic parameters.

Table 4 represents the evaluation criteria for both training and validation phases averaged over all subjects in predicting the kinematic parameters. The prediction error corresponding to displacement along the x-axis was larger compared to the other two kinematic parameters. Also, TDFOS and TDMLPANN outperformed TDLET in predicting the kinematic parameters. Moreover, to have a better comparison between methods, the average elapsed time for each method in training and validation phases is provided in Table 5. The training [validation] phase for TDFOS was approximately 122 [32] times as well as 2 [10] times faster compared to those of TDMLPANN [TDLET].

Fig. 9 indicates the average frequency of basis function selection for TDFOS over all subjects. Squared functions were selected less than 10% of the times. Hence, excluding them from the training phase would reduce the TDFOS training time by roughly 10% probably without degrading the model performance.

Since, we employed SEMG signals to predict the mandible movements, considering the performance of each subject's model over other subjects seems necessary. It was previously suggested [70], that a model identified for one subject may not be valid for another subject due to different reasons including differences in electrode positioning with respect to the muscles' motor points, the amount of tissue between the electrodes and muscles, and variable characteristics of muscle fibers, volume, and length. Here, we investigated the efficiency of our models trained on the signals obtained from one subject in predicting the output parameters corresponding to other subjects. In Fig. 10 the performance of the models is evaluated in terms of CC and AAE. Each bar represents the average of CC and AAE in predicting the dynamic parameters

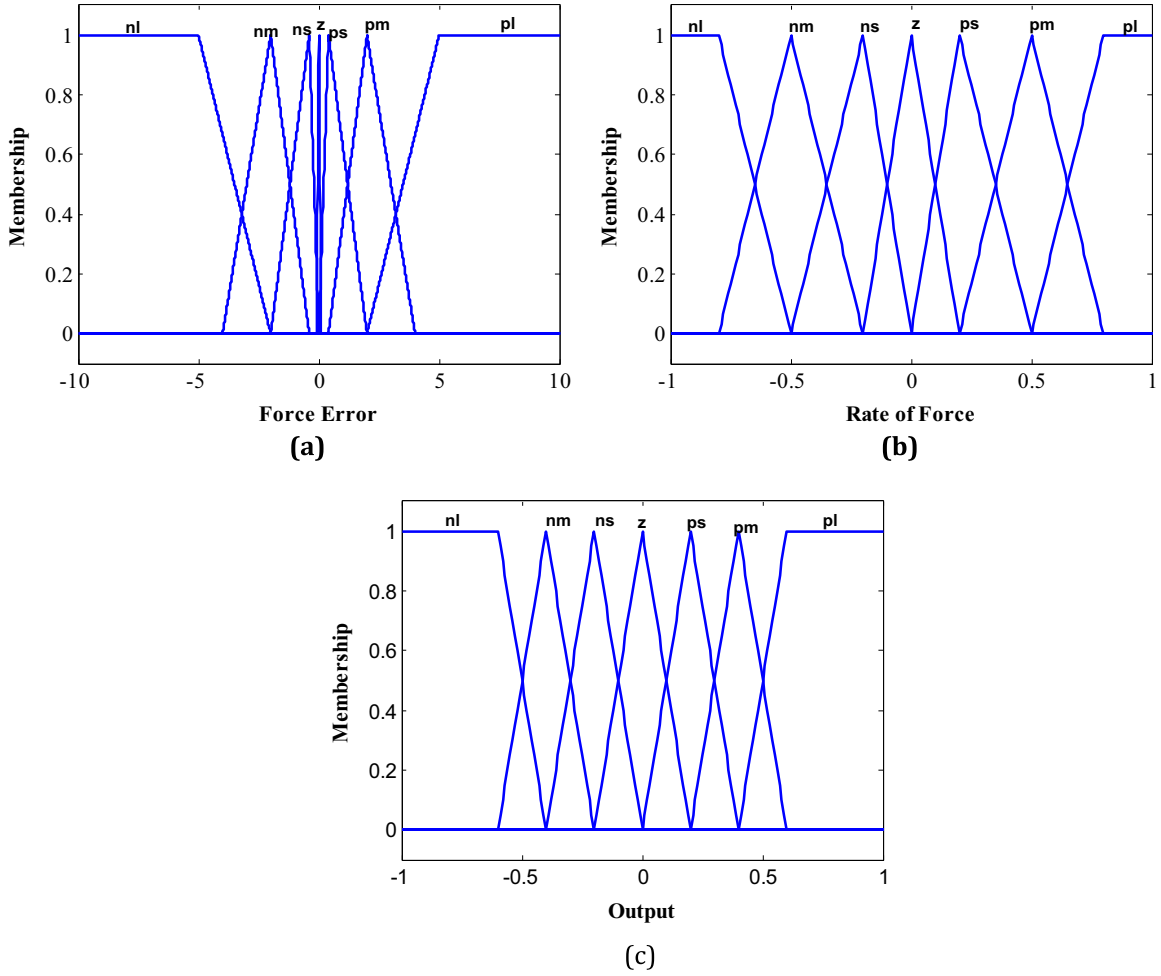

Fig. 7. Input–output membership functions. (a) force error, (b) rate of force and (c) Fuzzy output (filter gain).

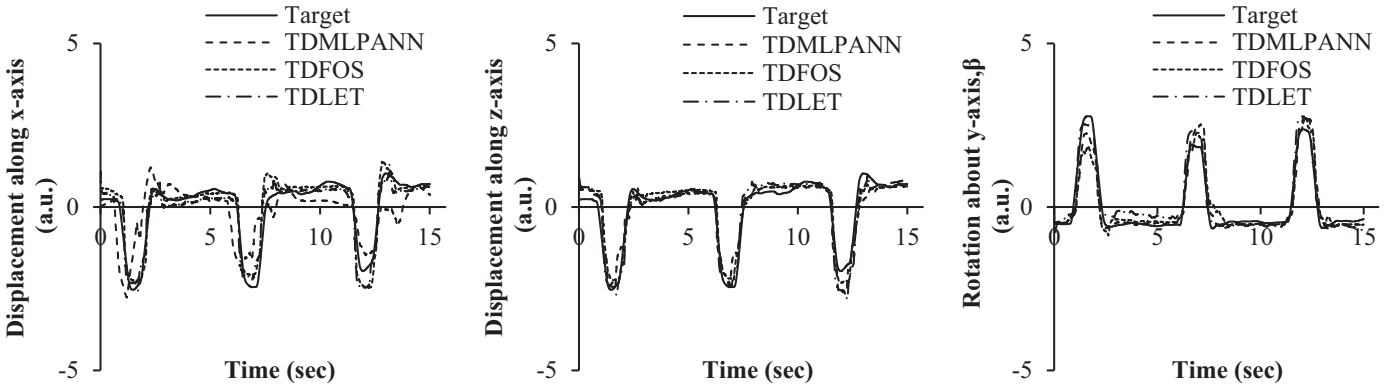

Fig. 8. Performance of models in predicting the three position/orientation kinematic parameters. All inputs and outputs were normalized as Z-score.

Table 4
Average and Standard deviation of RMSE, CC, AAE values for training and validation.

		Displacement, x-axis		Displacement, z-axis		Orientation, y-axis	
		Training	Validation	Training	Validation	Training	Validation
TDMLPANN	Average	25,86,0.4	44,73,0.4	7,97,0.2	14,94,0.2	12,96,0.2	22,90,0.3
	Standard deviation	17,10,0.1	24,16,0.1	4,1,0.1	6,2,0.05	13,2,0.1	10,4,0.092
TDFOS	Average	12,90,0.3	33,71,0.5	3,97,0.2	8,94,0.2	2,96,0.2	15,85,0.3
	Standard deviation	19,11,0.1	23,17,0.2	2,2,0.1	5,2,0.07	1,2,0.1	11,11,0.1
TDLET	Average	25,85,0.3	36,80,0.4	13,92,0.1	16,92,0.2	10,94,0.2	29,86,0.3
	Standard deviation	20,13,0.1	27,14,0.1	23,14,0.1	11,4,0.1	8,4,0.09	22,8,0.1

Table 5
Average of elapsed time for training and validation steps

Methods	Training (s)	Validation (s)
TDMLPANN	16.3	0.6
TDFOS	0.13	0.018
TDLET	0.24	0.17

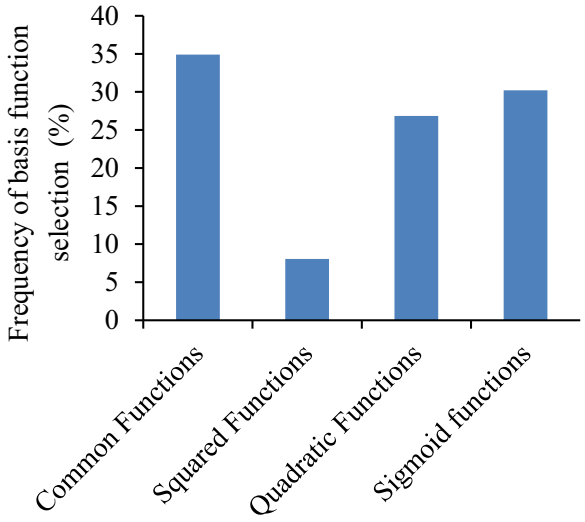

Fig. 9. The average frequencies by which each category of basis functions was selected.

of maximum jaw opening and closing across all seven subjects with the vertical bars indicating mean±standard deviation. TDFOS Performed better compared to the other two proposed methods. Also displacements along the z-axis and rotations about the y-axis were better predicted compared to displacement along the x-axis. From Fig. 10 it can be concluded that the performance of the identified models for displacement/rotation trained on the data from some of the subjects, e.g. subject 4, was superior to that of the models corresponding to other subjects.

One-way ANOVA (analysis of variance) and multiple comparisons were performed on three groups of predictions (position/orientation) to compare the performance of TDMLPANN, TDFOS and TDLET. The RMSE analysis statistically verified as significant for a p-value less than 0.05. The p-values for the three groups are shown in Table 6. In general, it was concluded that TDFOS provided lower RMSE compared to the other two methods mentioned above; the reduction was significant while compared to TDMLPANN in prediction of displacement along the x-axis ($p < 0.03$) and rotation about the y-axis ($p < 0.006$), while this did not hold for prediction of displacement along the z-axis ($p < 0.15$). Moreover, the error reduced from TDLET to TDMLPANN and TDFOS having a significant reduction in RMSE for all kinematic parameters.

3.2. SEMG-based fuzzy impedance control

The results up to this point demonstrate that the parameters corresponding to the static position and jaw movements during clenching can be predicted using the proposed models and SEMG signals. An SEMG-based Fuzzy impedance control scheme was later utilized for a masticatory rehabilitation robot. First the tele-operator's mandible motion required for clenching was estimated based on the SEMG signals. According to the previous reports (Table 6 and Fig. 10) on the performance of different modeling approaches, TDFOS was used to estimate the mandible movement for control purposes. Next, the robot was controlled in the desired trajectory. We evaluated the proposed architecture in a real-time test by simulating the rehabilitation robot in a tele-operation scenario (Fig. 6). The user was instructed to open and close his mandible. The SEMG signals of the two previously mentioned masticatory muscles were recorded and the rehabilitation robot tried to reconstruct the movement in the imaginary jaw in real time using the proposed control strategies. Fig. 11(a–c) shows the CP (on the moving platform) trajectory during the real operation. The jaw model was mounted on the robot merely to represent

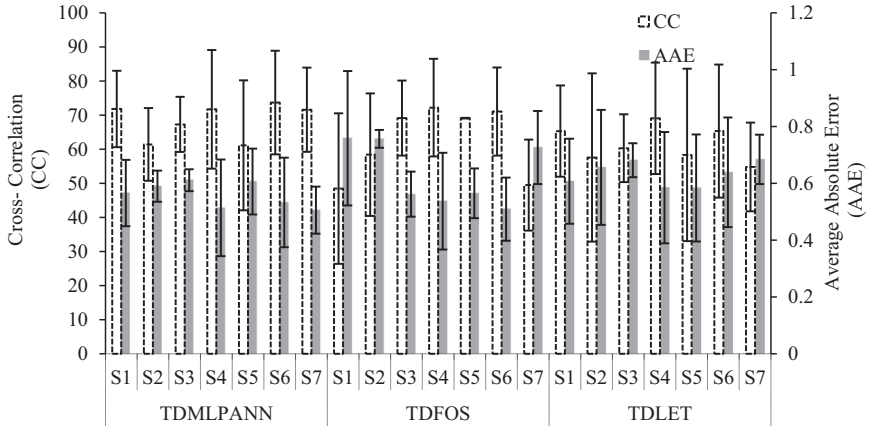

(a) Displacement along x-axis

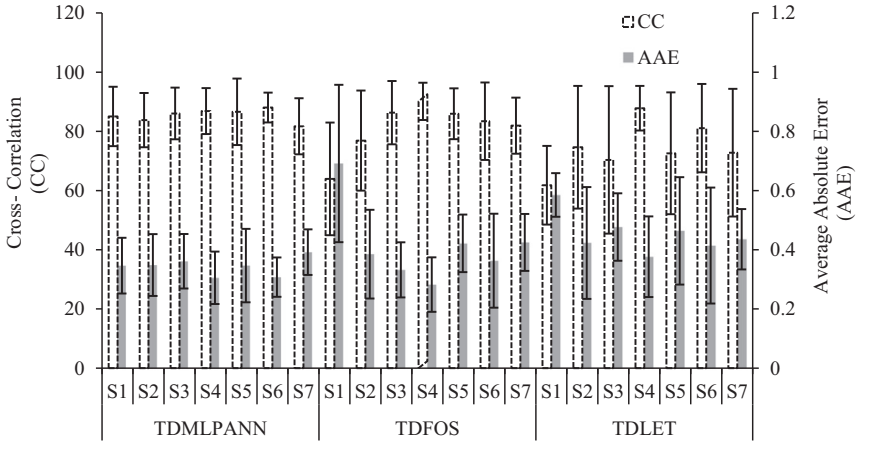

(b) Displacement along z-axis

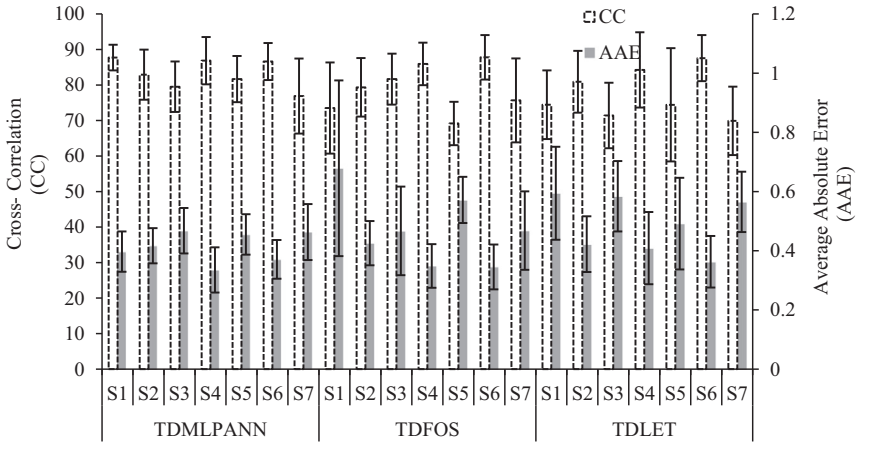

(c) rotation about y-axis

Fig. 10. Summary of CC and AAE in predicting the kinematic parameters. Models were trained based on the data corresponding to each subject. The evaluation criteria were averaged overall subjects, excluding the subject used for training. Error bars indicate ± standard deviation.

how the lengths of the actual masticatory muscles changed in time in response to the movements of the platform, and hence the chewing pattern. Fig. 11(d) shows that the Temporalis muscles experienced larger length variations compared to the Masseter and Pterygoid muscles. The Pterygoid muscles length experiences smaller variations compared to the other two aforementioned muscles. This is in agreement with previous results since Pterygoid muscles do not play a major role in the clenching movement [4].

For illustration purposes snapshots of the experiment, in which the robot legs and actual jaw muscles where controlled in real-time, are presented in Fig. 12. The variations in the position of CP in the simulator due to the movement of the platform are also presented in Fig. 12(b). While the mouth is closed the CP is located at $[x, y, z]$ or the origin of the coordinate system. During chewing the new coordinate of the CP is $[x',y',z']$ which varies due to the chewing patterns.

Table 6
The *p*-values for comparing the accuracy (in terms of RMSE) of all models. ± shows that the method in each row has a better/worse performance than the method in the corresponding column.

		Displacement along *x*-axis			Displacement along *z*-axis			Rotation about *y*-axis		
		TDMLPANN	TDFOS	TDLET	TDMLPANN	TDFOS	TDLET	TDMLPANN	TDFOS	TDLET
P-value	TDMLPANN	*	< 0.03 −	< 0.003 +	*	< 0.15 −	< 1.3e-5 +	*	< 0.006 −	< 0.07 +
	TDFOS	*	*	< 0.0007 +	*	*	< 0.0002 +	*	*	< 0.0005 +
	TDLET	*	*	*	*	*	*	*	*	*

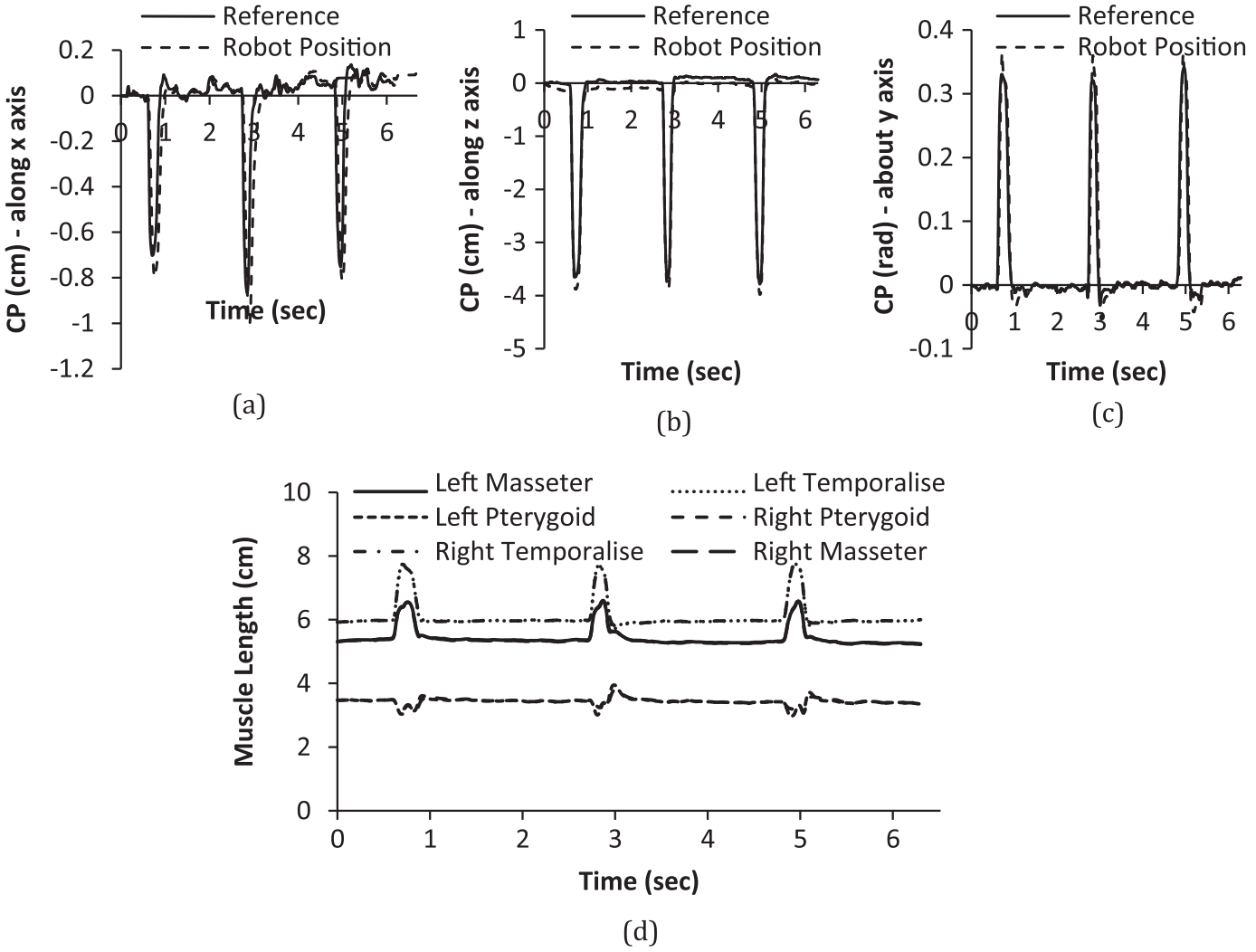

Fig. 11. CP trajectory (a) along *x*, (b) *z*, (c) and about the *y*-axis, (d) Time-varying lengths of muscles during the chewing pattern.

4. Discussion

The overall goal of this research was to develop a simple yet plausible methodology to provide a robot for masticatory rehabilitation purposes. We developed an SEMG-based model by means of which jaw opening and closing during the mastication process was reproduced. The results presented above indicate that if a gross prediction of the jaw motion is desired TDMLPANN, TDFOS and TDLET can predict the trajectory with reasonable accuracy using only SEMG signals. The predictions were less accurate during maximum jaw opening. TDFOS outperformed TDMLPANN and TDLET, although reduction in RMSE did not verify as significant for all cases, namely in comparison with TDMLPANN in predicting displacement along the *z*-axis (Tables 4 and 6). However, the training procedure for TDFOS was 122 and 2 times faster than that of TDMLPANN and TDLET (Table 5), respectively. The saved training time can be employed for checking the quality of recorded data and utilization of a more comprehensive control scheme.

As presented in Table 4 and Figs. 8, 10, and 11(a) predictions of displacement and robot tracking of the CP along the *x*-axis were less accurate compared to the other two parameters. This was perhaps due to the lower quality of motion data in this specific dimension.

A recent study [70] suggested that the identified model for one subject may not be valid for another subject. Discrepancies may be owing to differences between subjects in, for example, electrode positioning with respect to the motor points of the muscles, the amount of tissue between the electrodes and muscles, and characteristics of the muscles/muscle fibers. Also since each individual employs a different muscle contraction strategy for a similar masticatory task, it is not always possible to find a universal model for accurate trajectory

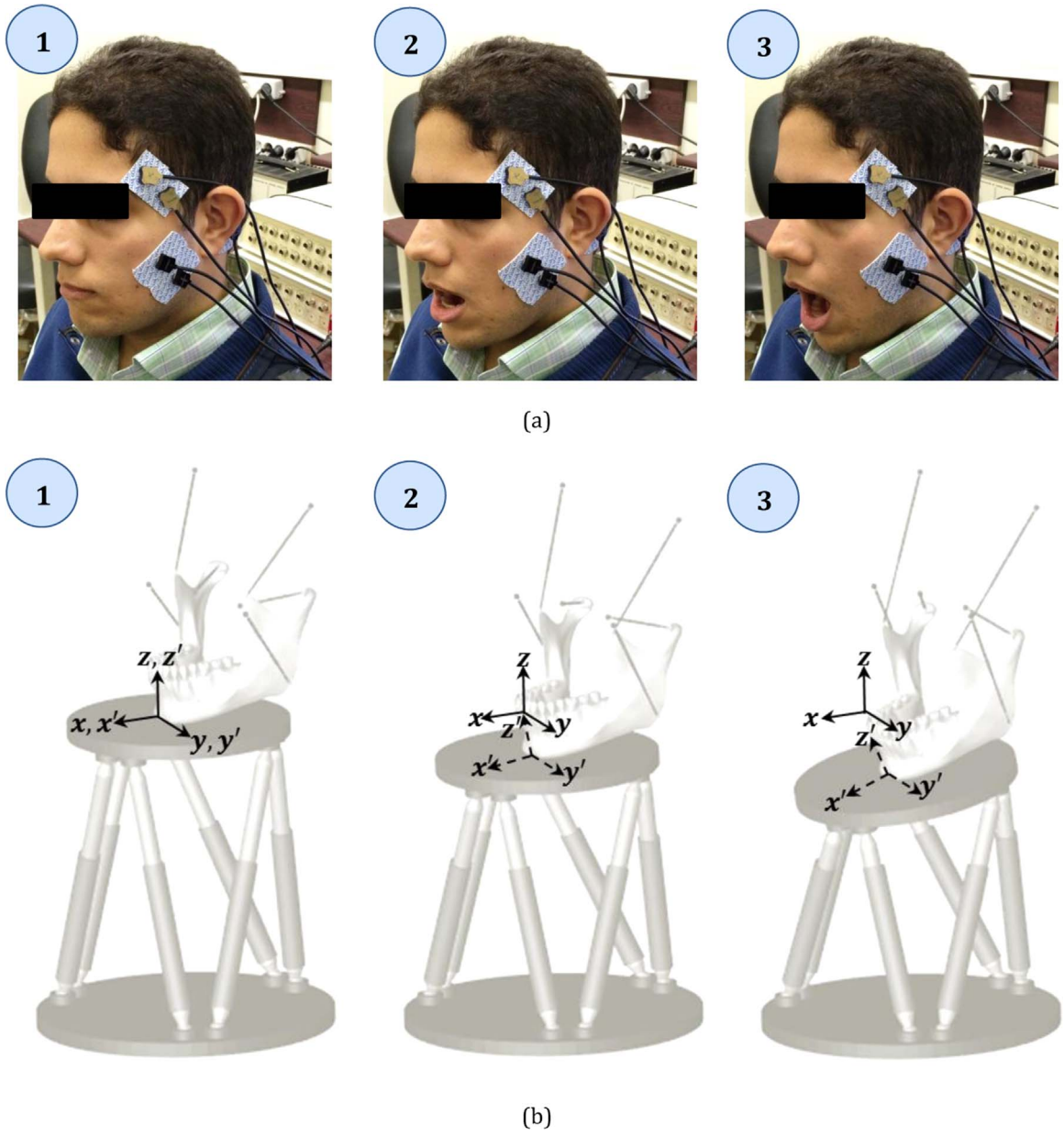

Fig. 12. Three postures of (a) user and (b) our model, during the chewing process. While the mouth is closed the CP is located at $[x, y, z]$ or the origin of the coordinate system. During chewing the new coordinate of the CP is $[x', y', z']$ which varies due to the chewing patterns.

prediction based on muscle activation [77]. As illustrated in Fig. 10, CC and AAE in predicting the kinematic parameters vary from one subject to another. Inter-subject variations of prediction accuracy could be owing to differences in jaw geometry, oral status, and other factors that were not considered in our model. Therefore, it is better to employ the GA method to find the best model structure for each subject separately.

A symmetric role was assumed for the masticatory muscles of healthy subjects in the defined task. However, as shown in Fig. 11 (d) muscle length variations of opposite muscles in the jaw model were not exactly alike. The reason for small differences is that no control in the direction of the y-axis was applied to the masticatory robot. This issue needs to be addressed when the desired motion is not limited to the frontal plane.

Although more than 20 muscles are involved in the process of human mastication, only six of these muscles play a major role [6], therefore, we chose to use a general 6-UPS parallel mechanism to represent the geometry of human mastication. We preferred to use the aforementioned mechanism rather than the previously recommended SPS (*Spherical-Prismatic-Spherical*) joints [3], for a few reasons. Compared to SPS joints, UPS joints provide a more realistic model of the muscle motion. 6-SPS provides six additional passive degrees of freedom, which allow in-place rotation of the leg about its own axis. However, this leg motion does not represent a realistic motion of the jaw muscle, also, according to the Chebyshev–Grübler–Kutzbach criterion, the six additional passive degrees of freedom in the legs in 6-SPS do not affect the kinematic input and output relationships of the manipulator, but they do increase the size of the dynamics equations [71].

This study was limited to clenching movements since considering the ethical issues we only used surface electrodes for recording the electrical activity of the muscles. Employing needle electrodes and recording the electrical activity of Pterygoid muscles can provide the required tools for predicting the lateral jaw motions during mastication. Moreover, since the Gough-Stewart parallel robot has six degrees of freedom it can cover the entire workspace of the human

masticatory process, hence having a more realistic reproduction of the system under study. In that case the same techniques which resulted in the masticatory robot presented in Fig. 12 can easily accommodate a combination of the new muscles along with the ones employed in the current study and therefore produce the desired chewing patterns.

In this work, a simple control interface was used, employing which, natural masticatory motion was produced in the patient's jaw with the help of a tele-operator. The gain of the impedance filter was adaptively changed using fuzzy rules and a reference force. Results show that the utilized control strategy can follow the reference force appropriately. In future studies the chance of operator's mistakes in producing unwanted movements with unsafe velocities has to be taken into consideration in designing the controllers.

5. Conclusions

This paper started with predicting the mandible movement during clenching based on SEMG signals and finishes with SEMG-based control of a rehabilitation robot. First, we investigated whether recorded the SEMG signals from voluntary muscles were sufficient for predicting the kinematics (position/orientation) of the mandible motion during clenching. Three different methods, TDMLPANN, TDFOS and TDLET were employed. In general, the results showed that: (1) the three modeling methods were capable of providing reasonably accurate estimations of the masticatory motion, (2) the accuracy and training/validation speed of TDFOS were higher than those of the other two aforementioned methods.

The fuzzy impedance scheme proved successful in controlling the moving platform for accurate navigation of the CP in the desired trajectory. SEMG has been widely used as a control command for prostheses and exoskeleton robots. However in the current study by employing the proposed rehabilitation robot the complete continuous profile of the masticatory motion was reproduced in the subject's jaw (using a simulator). After supplementary considerations regarding fixation of subject's head and jaw in the system as well as including chances of undesired movements in the control scheme, the proposed system can have the potential to be employed in masticatory rehabilitation programs.

The main contributions of this paper include implementing an online method where masticatory trajectory for a rehabilitation robot was generated in real-time by combining several concepts, tools and methods such as, direct and inverse kinematics, fuzzy impedance control and parametric and non-parametric models. Specifically, this paper contributes by (2) using TDMLPANN, TDFOS and TDLET to estimate the time-varying behavior of the kinematic parameters during clenching, (3) implementing the Fuzzy impedance scheme for control of a Gough-Stewart parallel robot as a masticatory rehabilitation robot based on the SEMG signals, (4) using one Gough-Stewart robot as a rehabilitation robot and another Gough-Stewart to model the human jaw, (5) developing a kinematic jaw model to demonstrate the time-varying behavior of the muscle lengths of subjects during a rehabilitation process.

Acknowledgments

The work described in this paper was supported by a Grant from the research office of Ferdowsi University of Mashhad (grant number 37133), Mashhad, Iran. We thank all the subjects who helped us by voluntarily participating in our study. The Authors thank Mr. Hassan Ghaderi from Motion Analysis Lab at the faculty of sports and physical education of Ferdowsi university of Mashhad for his assistance during the recording sessions.

Appendix A.1

To represent the geometry of human mastication, we use a general Gough-Stewart platform. The mobile and stationary platforms represent the human mandible and skull, respectively, and the actuators represent the jaw muscles (schematic in Fig. A1.1). Dimensions were chosen according to the available literature [4]. Actuators S_1 to S_6 in Fig. A1.1 represent the lateral Pterygoid, Temporalis, and Masseter muscles, respectively, and G_i and M_i ($i=1, 2,\ldots 6$) represent the connecting locations of these muscles to the skull and mandible. Table A1-1 shows the coordinates of these points [4]. The origin of the mandible system is located at the chewing point, CP, and its distance from the skull system is assumed to be [78.85 0 -81.87] mm [4].

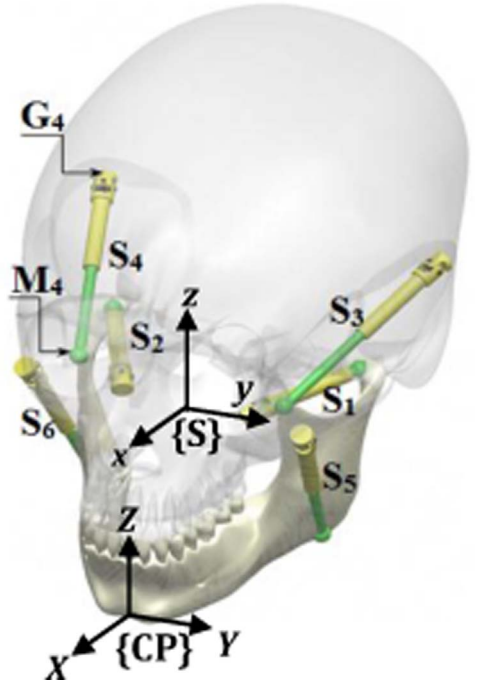

Fig. A1.1. The mandible, actuators and connecting points.

Table A1.1
Coordinate of muscle actuators (mm) and total actuator lengths (mm) [4].

Actuators	Coordinate of attaching points on the skull (mm)			Coordinate of attaching points on the mandible(mm)			Total actuator length (mm)
	x	*y*	*z*	*X*	*Y*	*Z*	
Masseter							
S_5	48.2	−52.5	−14.7	18	−44.7	−47.7	45.6
S_6	48.2	52.5	−14.7	18	44.7	−47.7	45.6
Temporalis							
S_3	13.3	−53.2	51.8	25.6	−43	2	52.2
S_4	13.3	53.2	51.8	25.6	43	2	52.2
Lateral Pterygoid							
S_1	21.5	−17.5	−12.4	−0.9	−41.1	−3.1	32.6
S_2	21.5	17.5	−12.4	−0.9	41.1	−3.1	32.6

Appendix A.2

To present rehabilitation robot, the Gough-Stewart platform is employed, which consists of a moving platform and a stationary base, connected to each other by six linear actuators. Consider Fig. A2.1. Frame {**T**} and frame {**O**} are attached to the moving platform and stationary base, respectively. Table A2.1 shows the physical parameters of the Rehabilitation robot.

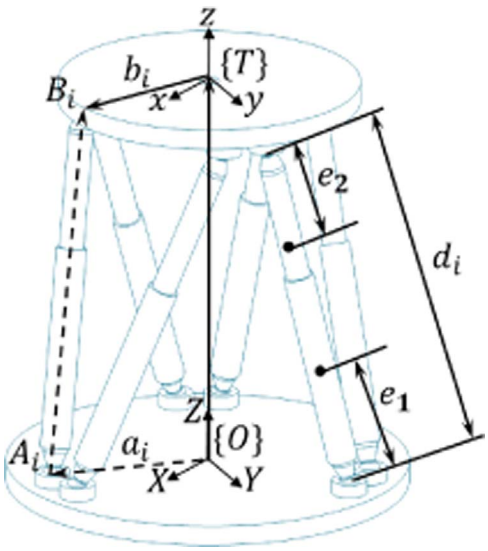

Fig. A2.1. The physical model and a closed loop vector for *i*th leg of the Rehabilitation robot.

Table A2.1
Physical parameters of the rehabilitation robot.

Position vectors of $\boldsymbol{A_i}$ joints on fixed and $\boldsymbol{B_i}$ joints on moving platform	
$a_1=[0.2831, 0.1489, -0.0780]^T$m	$b_1=[0.2883, 0.1152, 0.0814]^T$m
$a_2=[0.2675, 0.1573, -0.0780]^T$m	$b_2=[0.2142, 0.1347, 0.0814]^T$m
$a_3=[0.1755, 0.1009, -0.0780]^T$m	$b_3=[0.2020, 0.1223, 0.0814]^T$m
$a_4=[0.1759, 0.0532, -0.0780]^T$m	$b_4=[0.2222, 0.0484, 0.0814]^T$m
$a_5=[0.2708, 0.0317, -0.0780]^T$m	$b_5=[0.2390, 0.0440, 0.0814]^T$m
$a_6=[0.2859, 0.0410, -0.0780]^T$m	$b_6=[0.2929, 0.0985, 0.0814]^T$m
Gravity centers of cylinder and piston for all legs $e_1=0.04, e_2=0.036m$	
Mass of the moving platform, cylinder and piston for all legs $m_{MP}=1.5$kg$m_{cyl}=m_{pis}=0.1$kg	
Moments of inertia of cylinder and piston for all legs as well as the moving platform (in local frames) $\mathbf{I}_{MP}=\begin{bmatrix}0.08&0&0\\0&0.08&0\\0&0&0.08\end{bmatrix}$(kg.m^2), $\mathbf{I}_{cyl,i}=\begin{bmatrix}6.25&0&0\\0&6.25&0\\0&0&0\end{bmatrix}\times10^{-3}$(kg.m^2) $\mathbf{I}_{pis,i}=\begin{bmatrix}6.25&0&0\\0&6.25&0\\0&0&0\end{bmatrix}\times10^{-3}$(kg.m^2)	

References

[1] U. Posselt, Movement areas of the mandible, J. Prosthet. Dent. 7 (1957) 375–385.
[2] J.S. Pap, W.L. Xu, J. Bronlund, A robotic human masticatory system – kinematic simulations, Int. J. Intell. Syst. Technol. Appl. 1 (2005) 3–17.
[3] J.D. Torrance, kinematic, Motion Control and Force Estimation of a chewing robot of 6RSS parallel Mechanism Ph.D thesis, Massy University, Palmerston North, New Zealand, 2011.
[4] W. Xu, J.E. Bronlund, Mastication Robots: Biological Inspiration to Implementation, Springer-Verlag Berlin Heidelberg Press, 2010.
[5] R. González, I. Montoya, J. Cárcel, Review: the use of electromyography on food texture assessment, Food Sci. Technol Int. 7 (2001) 461–471.
[6] M.E. Wilson, J.R. Green, The development of jaw motion for mastication, Early Hum. Dev. 85 (2009) 303–311.
[7] J.R. Green, Orofacial movement analysis in infants and young children: new opportunities in speech studies, The Standard 2 (2002) 1–3.
[8] M.F. Kelly, P. Parker, R.N. Scott, The application of neural networks to myoelectric signal analysis: a preliminary study, IEEE Trans. Biomed. Eng. 37 (1990) 221–230.
[9] B. Hudgins, P. Parker, R.N. Scott, A new strategy for multifunction myoelectric control, IEEE Trans. Biomed. Eng. 40 (1993) 82–94.
[10] T. Tsuji, H. Ichinobe, K. Ito, M. Nagamachi, Discrimination of forearm motions from EMG signals by error back propagation typed neural network using entropy, Trans. Soc. Instrum. Control Eng. 29 (1993) 1213–1220.
[11] T. Tsuji, O. Fukuda, M. Kaneko, K. Ito, Pattern classification of time-series EMG signals using neural networks, Int. J. Adapt. Control Signal Process. 14 (2000) 829–848.
[12] H. Kalani, S. Moghimi, A. Akbarzadeh, SEMG-based prediction of masticatory kinematic in rhythmic clenching movements, Biomed. Signal Process, Control 20 (2015) 24–34.
[13] H. Kalani, A. Akbarzadeh, S. Moghimi, Prediction of jaw movements based on EMG signals using fast orthogonal search, Electr. Eng. (ICEE) (2015) 17–22.
[14] W.E. Brown, Method to investigate differences in chewing behaviour in humans: I. Use of electromyography in measuring chewing, J. Text. Stud. 25 (1994) 1–16.
[15] F.R. Jack, J.R. Piggott, A. Paterson, Relationships between electromyography, sensory and instrumental measures of cheddar cheese texture, J. Food Sci. 58 (1993) 1313–1317.
[16] W.E. Brown, K.R. Langley, L. Mioche, S. Marie, S. Gerault, D. Braxton, Individuality of understanding and assessment of sensory attributes of foods, in particular, tenderness of meat, Food Qual. Pref. 7 (1996) 205–216.
[17] D. Braxton, C. Dauchel, W.E. Brown, Association between chewing efficiency and mastication patterns for meat, and influence on tenderness perception, Food Qual. Pref. 7 (1996) 217–223.
[18] W.E. Brown, D. Braxton, Dynamics of food breakdown during eating in relation to perceptions of texture and preference: a study on biscuits, Food Qual. Pref. 11 (2000) 259–267.
[19] N. Bu, M. Okamoto, T. Tsuji, A hybrid motion classification approach for EMG-based human–robot interfaces using bayesian and neural networks, IEEE Trans Robot. 25 (2009) 502–511.
[20] L. Lucas, M. DiCicco, Y. Matsuoka, An EMG-controlled hand exoskeleton for natural pinching, J. Robot. Mechatron. 16 (2004) 482–488.
[21] D. Graupe, J. Magnussen, A.A.M. Beex, A microprocessor system for multifunctional control of upper limb prostheses via myoelectric signal identification, IEEE Trans. Autom. Control 23 (1978) 538–544.
[22] M. Zecca, S. Micera, M.C. Carrozza, P. Dario, Control of multifunctional prosthetic hands by processing the electromyographic signal, Crit. Rev. Biomed. Eng. 30 (2002) 459–485.
[23] O. Fukuda, T. Tsuji, M. Kaneko, A. Ohtsuka, A human-assisting manipulator teleoperated by EMG signals and arm motions, IEEE Trans. Robot. Autom. 19 (2003) 210–222.
[24] J. Hashemi, E. Morin, P. Mousavi, K. Mountjoy, K. Hashtrudi-Zaad, EMG–force modeling using parallel cascade identification, J. Electromyogr. Kinesiol. 22 (2012) 469–477.
[25] M.A. Oskoei, H. Hu, Myoelectric control systems – a survey, Biomed. Signal Process. Control 2 (2007) 275–294.
[26] M. Mulas, M. Folgheraiter, G. Gini, An EMG-controlled exoskeleton for hand rehabilitation, in: International Conference on Rehabilitation Robotics, 2005, ICORR 2005, June–1 July, p. 371–374, 2005.
[27] K. Kiguchi, T. Tanaka, T. Fukuda, Neuro-fuzzy control of a robotic exoskeleton with EMG signals, IEEE Trans. Fuzzy Syst. 12 (2004) 481–490.
[28] C.L. Pulliam, J.M. Lambrecht, R.F. Kirsch, Electromyogram-based neural network control of transhumeral prostheses, J. Rehabil. Res. Dev. 48 (2011) 739–754.
[29] R.N. Khushaba, S. Kodagoda, M. Takruri, G. Dissanayake, Toward improved control of prosthetic fingers using surface electromyogram (EMG) signals, Expert Syst. Appl. 39 (2012) 10731–10738.
[30] S. Kundu, K. Kiguch, Design and control strategy for a 5 DOF above-elbow prosthetic arm, Int. J. Assist. Robot. Mechatron. 9 (2008) 61–75.
[31] Gopura RARC, K. Kiguchi, Electromyography (EMG)-signal based fuzzy-neuro control of a 3 degrees of freedom (3DOF) exoskeleton robot for human upper-limb motion assist, J. Natl. Sci. Found. Sri Lanka 37 (2009) 241–248.
[32] J. Rafiee, M.A. Rafiee, F. Yavari, M.P. Schoen, Feature extraction of forearm EMG signals for prosthetics, Expert Systems with Applications 38 (2011) 4058–4067.
[33] J. Yousefi, A. Hamilton-Wright, Characterizing EMG data using machine-learning tools, Comput. Biol. Med. 51 (2014) 1–13.
[34] E. Hortal, D. Planelles, A. Costa, E. Iáñez, A. Úbeda, J.M. Azorín, E. Fernández, SVM-based brain-machine interface for controlling a robot arm through four mental tasks, Neurocomputing 151 (2015) 116–121.

[35] A. Subasi, Classification of EMG signals using PSO optimized SVM for diagnosis of neuromuscular disorders, Comput. Biol. Med. 43 (2013) 576–586.
[36] B. Blasberg, M. Greenberg, Temporomandibular disorders, Burket's Oral Med. Diagn. Treat. (2003) 271–306.
[37] C. McNeill, Management of temporomandibular disorders: concepts and controversies, J. Prosthet. Dent. 77 (1997) 510–522.
[38] A. Scherpenhuizen, M.A. Waes, M. Janssen, E. Cann, I. Stegeman, The effect of exercise therapy in head and neck cancer patients in the treatment of radiotherapy-induced trismus: a systematic review, Oral Oncol. 51 (8) (2015) 745–750.
[39] C. Lin, Y. Kuo, L. Lo, Design, manufacture and clinical, evaluation of a new TMJ exerciser, Biomed. Eng. Appl. Basis Commun. 17 (2005) 135–140.
[40] J. Krakauer, Motor learning: its relevance to stroke recovery and neurorehabilitation, Curr. Opin. Neurol. (2006) 94–103.
[41] V. Huang, J. Krakauer, Robotic neurorehabilitation: a computational motor learning perspective, J. NeuroEng. Rehabil. (2009) 1–13.
[42] G. Maloney, N. Mehta, A. Forgione, K. Zawawi, E. Al-Badawi, S. Driscoll, Effect of a passive jaw motion device on pain and range of motion in TMD patients not responding to flat plane intraoral appliances, Cranio 20 (2002) 55–66.
[43] L. Lo, C. Lin, Y. Chen, A device for temporomandibular joint exercise and trismus correction: design and clinical application, J. Plast. Reconstr. Aesthet. Surg. 61 (2008) 297–301.
[44] H. Takanobu, et al., Mouth opening and closing training with 6-DOF parallel robot, in: Proceedings of the 2000 IEEE International Conference on Robotics & Automation, San Francisco, pp. 1384–1389, 2000.
[45] H. Takanobu, et al., Jaw training robot and its clinical results, in: Proceedings of IEEE/ASME International Conference on Advanced Intelligent Mechatronics (AIM 2003), pp. 932–937, 2003.
[46] X.Y. Wang, W.L. Xu, Mechanism Design and Analysis of a Wearable Device for Rehabilitaion of Temporomandibular Disorder, in: Proceedings of the 2010 IEEE International Conference on Robotics and Biomimetics, China, pp. 1674–1679, 2010.
[47] M.D. Stubblefield, L. Manfield, E.R. Riedel, Preliminary report on the efficacy of a dynamic jaw opening device (dynasplint trismus system) as part of the multimodal treatment of trismus in patients with head and neck cancer, Arch. Phys. Med. Rehabil. 91 (8) (2010) 1278–1282.
[48] M. Cicciù, G. Cervino, E. Bramanti, F. Lauritano, G. Lo Gudice, L. Scappaticci, A. Rapparini, E. Guglielmino, G. Risitano, FEM analysis of mandibular prosthetic overdenture supported by dental implants: evaluation of different retention methods, Comput. Math. Methods Med. (2015), ID 943839.
[49] M. Cicciu, E. Bramanti, G. Matacena, E. Guglielmino, G. Risitano, FEM evaluation of cemented-retained versus screw-retained dental implant single-tooth crown prosthesis, Int. J. Clin. Exp. Med. 7 (4) (2014) 817–825.
[50] S. Oh, E. Baek, S. Song, S. Mohammed, D. Jeon, K. Kong, A generalized control framework of assistive controllers and its application to lower limb exoskeletons, Robot. Auton. Syst. 73 (2015) 68–77.
[51] K. Kiguchi, M. Rahman, M. Sasaki, K. Teramoto, Development of a 3DOF mobile exoskeleton robot for human upper-limb motion assist, Robot. Auton. Syst. 65 (2008) 678–691.
[52] S. Mefoued, A second order sliding mode control and a neural network to drive a knee joint actuated orthosis, Neurocomputing 155 (2015) 71–79.
[53] E. Rechy-Ramirez, H. Hu, Bio-signal based control in assistive robots: a survey, Digit. Commun. Netw. 1 (2015) 85–101.
[54] D. Yang, J. Zhao, Y. Gu, X. Wang, N. Li, L. Jiang, H. Liu, H. Huang, D. Zhao, An anthropomorphic robot hand developed based on under actuated mechanism and controlled by EMG signals, J. Bionic Eng. 6 (2009) 255–263.
[55] E. Kamavuako, E. Scheme, K. Englehart, On the usability of intramuscular EMG for prosthetic control: a Fitts' law approach, J. Electromyogr. Kinesiol. 24 (2014) 770–777.
[56] K. Xing, P. Yang, J. Huang, Y. Wang, Q. Zhu, A real-time EMG pattern recognition method for virtual myoelectric hand control, Neurocomputing 136 (2014) 345–355.
[57] M.S. Ju, C.C.K. Lin, S.M. Chen, I.S. Hwang, P.C. Kung, Z.W. Wu, Applications of Robotics to Assessment and Physical Therapy of Upper Limbs of Stroke Patients, Rehabilitation Robotics, Sashi S. Kommu (Ed.), ISBN: 978-3-902613-04-2, InTech.
[58] N. Hogan, Impedance control an approach to manipulation: part i-theory, part ii-implementation, part iii-applications, J. Dyn. Syst. Meas. Control 107 (1985) 1–24.
[59] H. Kazerooni, Robust, non-linear impedance control for robot manipulators, Robotics and Automation. Proceedings. 1987 IEEE International Conference on, pp. 741–750.
[60] H. Seraji, R. Colbaugh, Force tracking in impedance control, Int. J. Robot. Res. 16 (1997) 97–117.
[61] S. Jung, T.C. Hsia, R.G. Bonitz, Force tracking impedance control of robot manipulators under unknown environment, IEEE Trans. Control Syst. Technol. 12 (2004) 474–483.
[62] S. Kizir, Z. Bingül, Fuzzy impedance and force control of a Stewart platform, Turk. J. Electr. Eng. Comput. Sci. 22 (2014) 924–939.
[63] Y. Li, S.S. Ge, Force tracking control for motion synchronization in human-robot collaboration, Robotica (2014) 1–22, http://dx.doi.org/10.1017/S0263574714002240.
[64] Korenberg, J. Michael, Parallel cascade identification and kernel estimation for nonlinear systems, Ann. Biomed. Eng. 19 (1991) 429–455.
[65] Korenberg, J. Michael, Fast orthogonal algorithms for nonlinear system identification and time-series analysis, Adv. Methods Physiol. Syst. Model. 2 (1989) 165–177.
[66] V.Z. Marmarelis, Nonlinear Dynamic Modeling of Physiological Systems, Wiley-IEEE Press, 2004.
[67] V.Z. Marmarelis, Identification of nonlinear biological systems using Laguerre expansions of kernels, Ann. Biomed. Eng. 21 (1993) 573–589.
[68] N. Goharian, S. Moghimi, H. Kalani, Estimation biting force based using EMG signals and laguerre estimation technique, ICEE (2015) 50–55.
[69] L.W. Tsai, Solving the inverse dynamics of Stewart-Gough manipulator by the principle of virtual work, J. Mech. Des. 122 (2000) 3–9.
[70] L. Ljung, System Identification, John Wiley & Sons Inc, 1999.
[71] H. Kalani, A. Rezaei, A. Akbarzadeh, Improved general solution for the dynamic modeling of gough-stewart platform based on principle of virtual work, Nonlinear Dyn. (2015), http://dx.doi.org/10.1007/s11071-015-2489-z (accepted).
[72] H. Kalani, A. Akbarzadeh, A. Mousavi, Fuzzy impedance control strategy for jaw rehabilitation using 6-UPS stewart robot, ICROM (2015) 2015.
[73] C. Luca, The use of surface electromyography in biomechanics, J. Appl. Biomech. 13 (1997) 135–163.
[74] T.S. Buchanan, D.G. Lloyd, Manal Kurt, T.F. Besier, Neuromusculoskeletal modeling: estimation of muscle forces and joint moments and movements from measurements of neural command, J. Appl. Biomech. 20 (4) (2004) 367–395.
[75] M. Croix, Y. ElNagar, J. Iga, D. James, F. Ayala, Electromechanical delay of the hamstrings during eccentric muscle actions in males and females: Implications for non-contact ACL injuries, J. Electromyogr. Kinesiol. 25 (2015) 901–906.
[76] F. Esposito, E. Cè, S. Rampichini, E. Limonta, M. Venturelli, E. Monti, L. Bet, B. Fossati, G. Meola, Electromechanical delay components during skeletal muscle contraction and relaxation in patients with myotonic dystrophy type 1, Neuromuscul. Disord. 26 (2016) 60–72.
[77] J.H. Koolstra, T.M. van Eijden, A method to predict muscle control in the kinematically and mechanically indeterminate human masticatory system, J. Biomech. 34 (2001) 1179–1188.